# Search for $CP$ Violation in $D^0/\overline{D^0} \to K^0_S\pi^0$, $K^0_SK^0_S$, $\pi^0\pi^0$ Decays

Larry Borum

*Physics Department, Wayne State University, Detroit, Michigan, 48202*

Maureen Gramaglia

*Physics Department, Pennsylvania State University, State College, Pennsylvania, 16802*

## Abstract

We report on a study of the asymmetries in the charm system in the decays of $D^0$ and $\overline{D^0}$ mesons to the CP eigenstates $K^0_S\pi^0$, $K^0_SK^0_S$, and $\pi^0\pi^0$. We used the strong interactions $D^{*+} \to D^0\pi^+_{slow}$ and $D^{*-} \to \overline{D^0}\pi^-_{slow}$ to differentiate between $D^0$ and $\overline{D^0}$ mesons. Our findings for the asymmetry in each decay mode, a measure of CP violation in this system, were all consistent with zero.

## Introduction

All known subatomic particles are paired with corresponding antiparticles. From this pairing, we might expect to have symmetry with respect to matter and antimatter. Scientists have theorized that early in the existence of the universe there was only a slight difference in amounts of matter and antimatter. Today antimatter is found only in cosmic rays and particle accelerators. To explain the absence of so much antimatter, theories propose that antimatter might decay at a faster rate than matter. This proposed contradiction to the rule of particle-antiparticle symmetry is a phenomenon called CP violation.[1]

C and P (separately) represent symmetries. C stands for charge conjugation or simply put, particle-antiparticle interchange. P represents parity or space inversion. These symmetries hold for strong and electromagnetic interactions, but not for weak interactions. After the discovery of large C and P violation in the weak interactions, it appeared that the product CP was a good symmetry. However, if matter decays one way, and antimatter another, CP would also be violated. We look for CP violation because we believe we know by how much CP should be violated. If experimental data shows otherwise, it could be a sign of new physics at work. To date, the only experimental evidence for CP violation is in the kaon system.

In this paper we report on a search for CP violation in the charm system. We looked for an asymmetry in the decay rates of the $D^0$ meson and its antiparticle, the $\overline{D^0}$ , arriving at the same CP eigenstates. This asymmetry was defined as

$$A = \frac{N(D^0) - N(\overline{D^0})}{N(D^0) + N(\overline{D^0})}, \tag{1}$$

where $N(D^0)$ ($N(\overline{D^0})$) refers to the number of $D^0$ ($\overline{D^0}$) mesons that decay to the same final state. A difference in the decay rates of the $D^0$ and $\overline{D^0}$ would represent a measure of CP violation. We studied decays to the CP eigenstates $K^0_S\pi^0$ , $K^0_SK^0_S$ , and $\pi^0\pi^0$ . We used only $D^0$ mesons that came from $D^{*+}$ mesons in the decay $D^{*+} \to D^0\pi^+_{slow}$ in order to exploit the

fact that the charge of the pion from this decay tells us whether we had a $D^0$ or $\overline{D^0}$ . (Charge conjugate particles are implied unless explicitly stated otherwise.)

$$D^0/\overline{D^0} \to K^0_S\pi^0$$

The first signal mode we will discuss is $K^0_S\pi^0$ . In order to perform the calculation of the asymmetry in the decay rates of $D^0$ and $\overline{D^0}$ mesons going to the same final state, we had first to identify the events in the data that we actually wanted to study. We wanted to select events where the $D^0$ was formed in the decay $D^{*+} \to D^0\pi^+_{\rm slow}$ and then decayed to the final state $K^0_S\pi^0$ . We didn't immediately begin looking for our signal events in real data gathered during collisions of $e^+$ and $e^-$ beams with a total center-of-mass energy of 10.58 GeV by the CLEOII and CLEOII.V detectors at the Cornell Electron Storage Ring (CESR). Instead, we began our analysis by studying simulated data. This approach had two main advantages. First, it gave us an opportunity to develop and polish our analysis in a setting where we already knew what particles were in the events, and what the asymmetry should be (the Monte Carlo simulation data was created to have zero asymmetry). Second, we avoided biasing our results by unconsciously finessing the real data to give a desired result. By studying 15.13 $fb^{-1}$ of simulated Monte Carlo data (5.99 $fb^{-1}$ of simulated CLEOII data and 9.14 $fb^{-1}$ of simulated CLEOII.V data) we were able to determine our selection criteria for the $K^0_S$, $\pi^0$, $D^0$, and $\pi^+_{\rm slow}$ . We chose our selection criteria, or cuts, based on how well they suppressed background while maintaining a good signal efficiency.

Several detector components were vital for this analysis. The first was a tracking system, which consists of a six-layer straw tube chamber, referred to as the PT Straw Chamber; a ten-layer vertex drift chamber; and a 51-layer main drift chamber. These three chambers combine to be called the Central Detector. There is also an electromagnetic calorimeter with 7800 CsI crystals. All of these components operate within a 1.5-Tesla solenoidal magnet. (In CLEOII.V the PT was replaced by a silicon vertex detector.) Measurements obtained from the various parts of the detector were converted into useful variables which could be studied and constrained to obtain a clean signal.

Our selection criteria for the $D^0$ , $K^0_S$ , and $\pi^0$ were based on the fact that all these particles have finite lifetimes. The $D^0$ decays to $K^0_S\pi^0$ or some other mode, the $K^0_S$ decays to $\pi^+\pi^-$, and the $\pi^0$ decays to two photons. Our first selection criteria were based on the candidate masses of the particles, and were fundamentally similar. In order to select the $K^0_S\pi^0$ mode and reduce background, we wanted to limit the mass of each candidate particle to be within a certain range of the previously measured or "known" mass of the particle. We determined how wide to make this range for each candidate mass distribution by looking only at signal events (using information from the simulation), and fitting the signal peak to a Gaussian function. The standard deviation $\sigma$ of the Gaussian gave a measure of the width of the signal peak. We then required the difference between the candidate mass and the known mass for the $D^0$ meson, $K^0_S$ , and $\pi^0$ to be about 2.5 to $3\sigma$. The more standard deviations wide our range was, the less signal would be excluded. The amount of background we had determined how tight our mass selection window must be. For example, we could afford to apply a wider window for the $K^0_S$ mass because our other selection requirements greatly reduced the amount of background.

Fig. 1, the $K^0_S$ candidate mass after all our other selection criteria were applied, illustrates

the procedure just described. The standard deviation for the signal peak was 3 MeV; we constrained the candidate mass to fall within 9 MeV, or $3\sigma$, of the known $K^0_S$ mass, 497.67 MeV.[2] The vertical lines on Fig. 1 illustrate the edges of the mass window. Because the background was already so far reduced by other selection criteria, we could afford this wide mass window. Based on these same principles, we limited the $\pi^0$ candidate mass to fall within 18 MeV of the known mass of 134.98 MeV, and the $D^0$ candidate mass to fall within 50 MeV of the known mass of 1.8645 GeV.

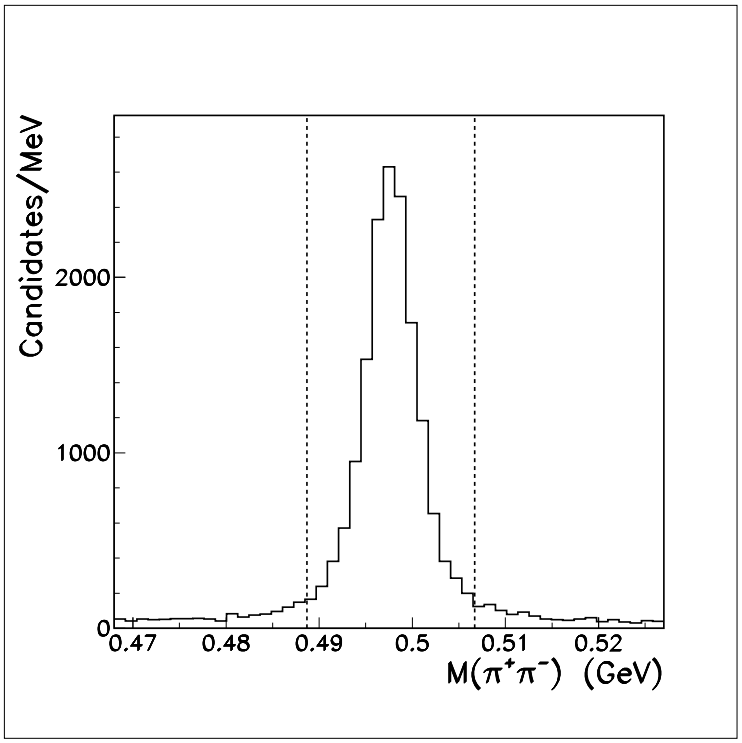


FIGURE 1. This is a plot of the candidate mass of the $K^0_S$ , in GeV, after all the other selection criteria were applied. The vertical lines indicate the edges of the mass window.

Next, we defined the decay angle as the angle $\theta$ between the $D^0$ momentum and the $K^0_S$ momentum in the $D^0$ rest frame. The $D^0$ has no intrinsic angular momentum (spin), and therefore it does not have a preferred direction of decay. The decay products $K^0_S$ and $\pi^0$ can be emitted in any direction, so the cosine of the decay angle should be evenly distributed between -1 and 1 for our signal events.

Background to our signal mode should peak at $\cos\theta = 1$. This effect is illustrated by Fig. 2, a plot of the absolute value of the cosine of the decay angle, after all our other selection criteria were applied. The solid line represents background events, and the dashed line represents signal events. (We used information from the simulation to generate this illustration.) The background peaks at $\cos\theta = 1$ because there are a lot of low momentum fake $\pi^0$ candidates. This background shows up, due to momentum conservation, as fast $K^0_S$ candidates. A fast $K^0_S$ candidate corresponds to a small decay angle; it would have to be traveling in almost the same direction as the $D^0$. This useful effect provides a way to eliminate a large number of background events. By requiring the cosine of the decay angle

to be less than 0.95, we eliminated a large amount of background without sacrificing too much signal. This requirement is illustrated by the vertical line in Fig. 2.

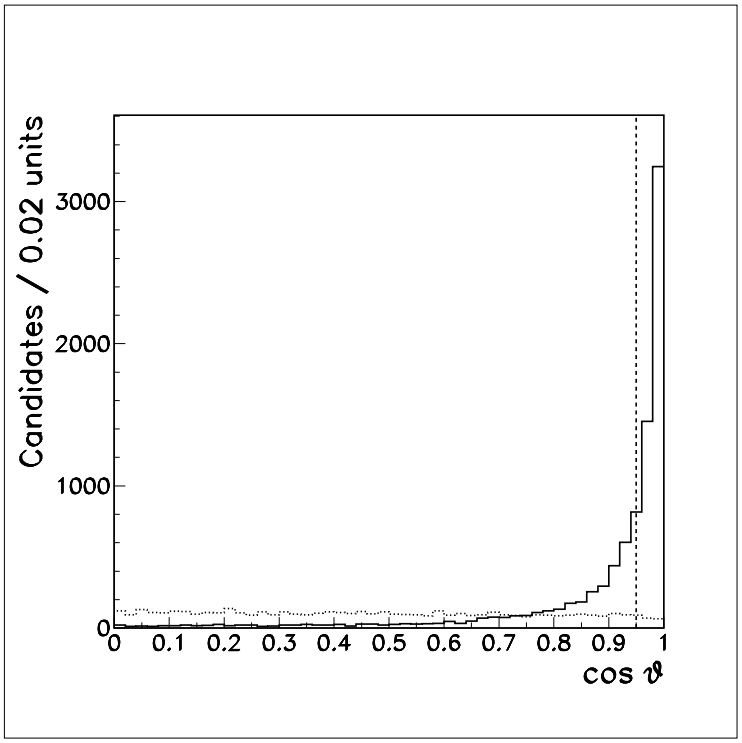


FIGURE 2. This is a plot of the absolute value of the cosine of the decay angle for the $K^0_S$. The solid line represents background events, and the dashed line represents signal events. The vertical dashed line indicates where we placed our cut, at 0.95.

We then further exploited the fact that the $K^0_S$ has a finite lifetime. Since we reconstructed the decay products, we could obtain a measure of the distance the particle traveled from the beam spot (where we assume it was formed) before it decayed. A vast amount of background to the $K^0_S$ is due to very unstable particles that decay very soon after they are formed. We can measure their decay lengths with the associated uncertainties. These background particles have very short decay lengths, so the ratio of their decay lengths to their uncertainties should be small. In fact, the ratio can even be negative when the resolution and the decay length are comparable. We call this ratio the significance of the decay length. In contrast, while the significance of the decay length of the $K^0_S$ also peaks at low values, the $K^0_S$ can also have longer decay lengths. Therefore, if we only accept candidate $K^0_S$ with a significance of decay length above a certain level, we will cut out a large amount of background and only some signal.

This is illustrated by Fig. 3. The solid line in the figure shows the significance of decay length for background $K^0_S$ candidates after the mass and decay angle cuts; the dashed line shows the distribution for signal $K^0_S$ candidates. We can see that while both signal and background peak at low significance of decay length, the peak for the background is much narrower and higher; it also has negative values. The vertical line illustrates that we required our $K^0_S$ candidates to have a significance of decay length greater than 3, thus removing a

large amount of background and a relatively small amount of signal.

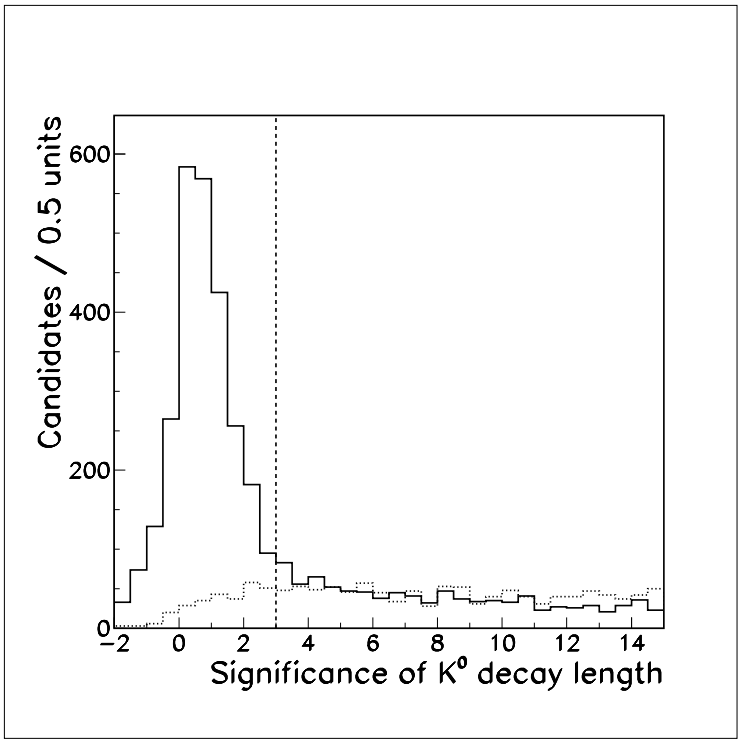


FIGURE 3. This is a plot of the significance of the decay length of the $K^0_S$ . The solid line represents background events, and the dashed line represents signal events. The vertical dashed line indicates where we placed our cut, at 3.0.

Our final $K^0_S$ selection criterion was related to the one based on significance of decay length. We think that a good $K^0_S$ candidate should have a well-defined decay vertex where it decayed into its daughters $\pi^+\pi^-$. When tracks are fit for the daughters, they should come from that decay vertex. It is possible, though, that tracks of particles that came from the interaction point could intersect, creating a fake vertex.

The $\chi^2$ of a $K^0_S$ candidate daughter to come from the beam spot is a measure of how well its track points back to the interaction point. A low value of $\chi^2$ indicates that the track, when extrapolated back toward the interaction point, seems to come from the interaction point. Of course, a low $\chi^2$ value is not a fool-proof way of identifying background; the track might by chance happen to point back to the beam spot when it really came from a decay vertex. However, as illustrated by the solid line in Fig. 4, a plot of the $\chi^2$ of a $K^0_S$ candidate daughter to come from the beam spot after the mass and decay angle cuts, the background does indeed peak at low values; the signal is more level, as shown by the dashed line in the same figure. This is true for both daughters of the $K^0_S$ . Therefore, as indicated by the vertical line in Fig. 4, we require the $\chi^2$ function to be greater than 2.5 for both daughters of the $K^0_S$ .

Once we selected our $\pi^0$, $K^0_S$, and $D^0$ (the selection criteria are summarized in Table 1), we turned to selecting the $\pi^+_{\rm slow}$. The $\pi^+_{\rm slow}$ are important because their charge indicate whether the event had a $D^0$ or a $\overline{D^0}$. The most crucial element of our $\pi^+_{\rm slow}$ selection was that it be

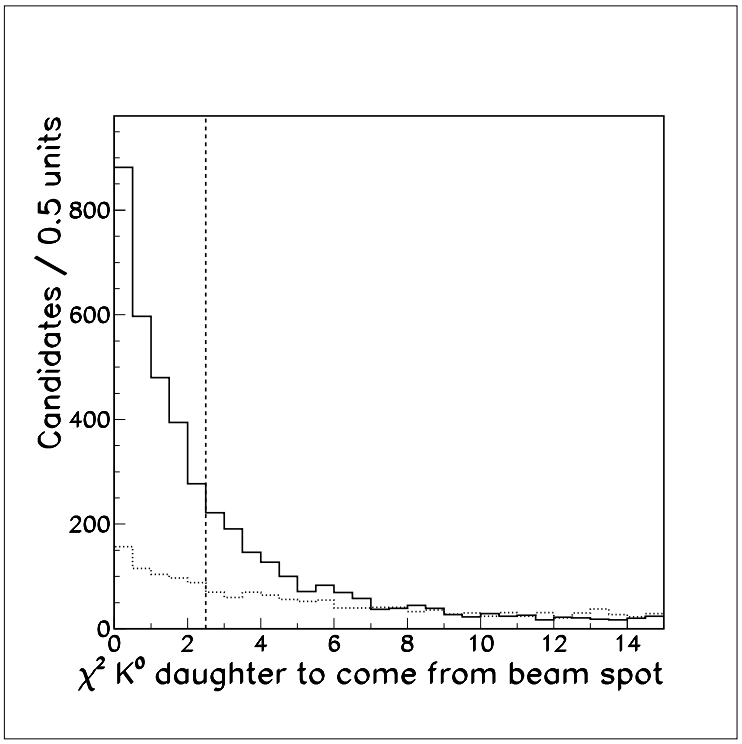


FIGURE 4. This is a plot of the $\chi^2$ of a $K^0_S$ candidate daughter to come from the beam spot. The solid line represents background events, and the dashed line represents signal events. The vertical dashed line indicates where we placed our cut, at 2.5 for both daughters.

TABLE 1. The selection criteria for the three $D^0$ decay modes. $\Delta M_x$ denotes the magnitude of the deviation of the invariant mass of the candidate $x$ from the known mass of $x$; for example, $\Delta M_\pi \equiv |M(\gamma\gamma) - M_{\pi^0}|$. The decay angle $\theta_d$ is defined as the angle between the $\pi^0(K^0_S)$ and $D^0$ candidate directions in the $D^0$ rest frame for the $\pi^0\pi^0(K^0_S\pi^0$ and $K^0_SK^0_S)$ decay modes. $L/\sigma(L)$ is the decay length significance of the $K^0_S$ candidate described in the text and $\chi_\pi$ is the minimum of the $\chi^2$ for either one of the $K^0_S$ daughter pions to come from the interaction point.

| | $D^0$ decay mode | | |
|---|---|---|---|
| Quantity | $K^0_S\pi^0$ | $\pi^0\pi^0$ | $K^0_SK^0_S$ |
| $\Delta M_\pi$ (MeV) | $< 18$ | $< 20$ | |
| $\Delta M_K$ (MeV) | $< 9$ | | $< 8$ |
| $\Delta M_D$ (MeV) | $< 50$ | $< 65$ | $< 18$ |
| $\cos\theta_d$ | $[-1.00, 0.95]$ | $[-0.875, 0.875]$ | $[-0.96, 0.96]$ |
| $L/\sigma(L)$ | $> 3$ | | $> 3$ |
| $\chi_\pi$ | $> 2.5$ | | $> 2.0$ |

unbiased; any bias that would cause us to detect more pions of one charge than the other could create a false asymmetry.

Two sorts of "false" tracks that could bias our $\pi^+_{\rm slow}$ selection were "ghost" tracks and "looping" tracks. "Ghosts" are false invalid tracks with trajectories very similar to the correct track but containing only a fraction of the central detector hits. Helical trajectories resulting from low momentum tracks ($\leq 200MeV$) will appear as "loops" in the detector; selecting the detector hits corresponding to the outgoing trajectory insures that the correct charge will be assigned to the reconstructed track. CLEO software analyzes the tracks to classify and select the correct track.

The other selection criteria were based on how well the track was fit based on the hits the $\pi^+_{\rm slow}$ made in the detector. They were determined in the same way as those for the $\pi^0$, $K^0_S$ and $D^0$ – by looking for a peak in the background where the signal was relatively low. The sum of the residuals of the track fit, an indicator of how well the path was reconstructed, was constrained to fall between $10^{-6}$ and $10^{-3}$ meters, inclusive. This variable is plotted in Fig. 5 for signal (dashed line) and background (solid line); the vertical line shows the upper limit of our selected region. The absolute value of the distance of closest approach of the track to the interaction point in the $r\phi$ plane was required to be less than 3 mm, and the absolute value of the distance of closest approach along the $z$ axis had to be less than 5 cm; these variables indicated how well the $\pi^+_{\rm slow}$ was fit to come from the interaction point. Fig. 6 illustrates the absolute value of the distance of closest approach in $r\phi$, and Fig. 7 illustrates the absolute value of the distance of closest approach in $z$. This set of selection criteria allowed us to obtain an essentially unbiased sample of $\pi^+_{\rm slow}$ (see section on Systematic Uncertainty).

Once the selection criteria for the $K^0_S$, $\pi^0$, $D^0$, and $\pi^+_{\rm slow}$ were established, the next step was to select $D^0$ that actually came from a $D^{*+}$. To accomplish this, we looked at a quantity called $Q$, the energy released in the $D^{*\pm}$ decay. $Q$ is defined by the expression

$$Q \equiv M(K^0_S\pi^0\pi^+_{\rm slow}) - M(K^0_S\pi^0) - M_{\pi^+}, \tag{2}$$

where $M(K^0_S\pi^0\pi^+_{\rm slow})$ is the total invariant mass of the $K^0_S$, $\pi^0$, and $\pi^+_{\rm slow}$ candidates (the candidate mass of the $D^{*+}$); $M(K^0_S\pi^0)$ is the total invariant mass of the $K^0_S$ and $\pi^0$ candidates

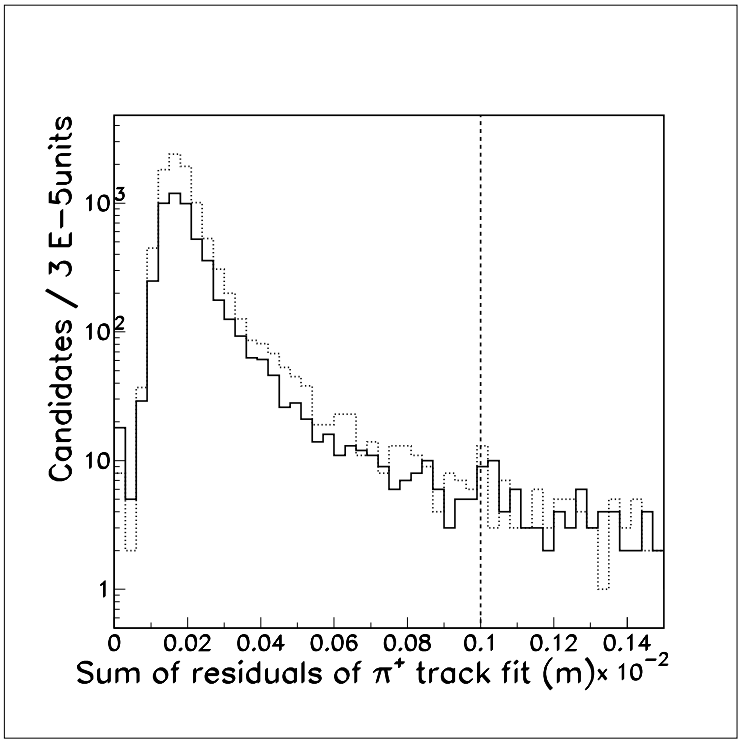


FIGURE 5. This is a plot of the sum of the residuals of the track fit for the $\pi^+_{\rm slow}$, in meters. The solid line represents background events, and the dashed line represents signal events. The vertical dashed line indicates the upper limit of our selected region, $10^{-3}$ m. The lower limit was $10^{-6}$ m.

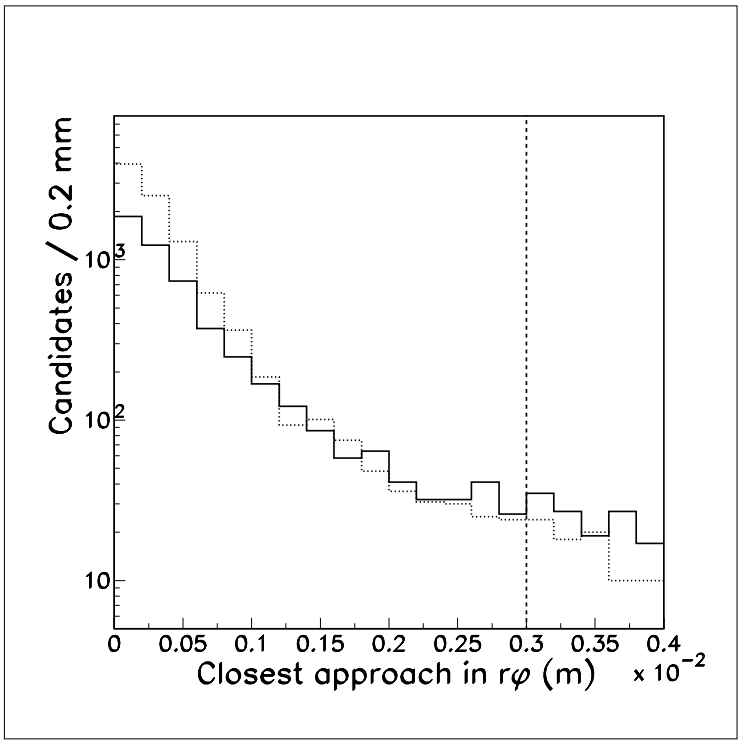


FIGURE 6. This is a plot of the absolute value of the distance of closest approach of the track to the interaction point in the $r\phi$ plane, in meters. The solid line represents background events, and the dashed line represents signal events. The vertical dashed line indicates where we placed our cut, at 3 mm.

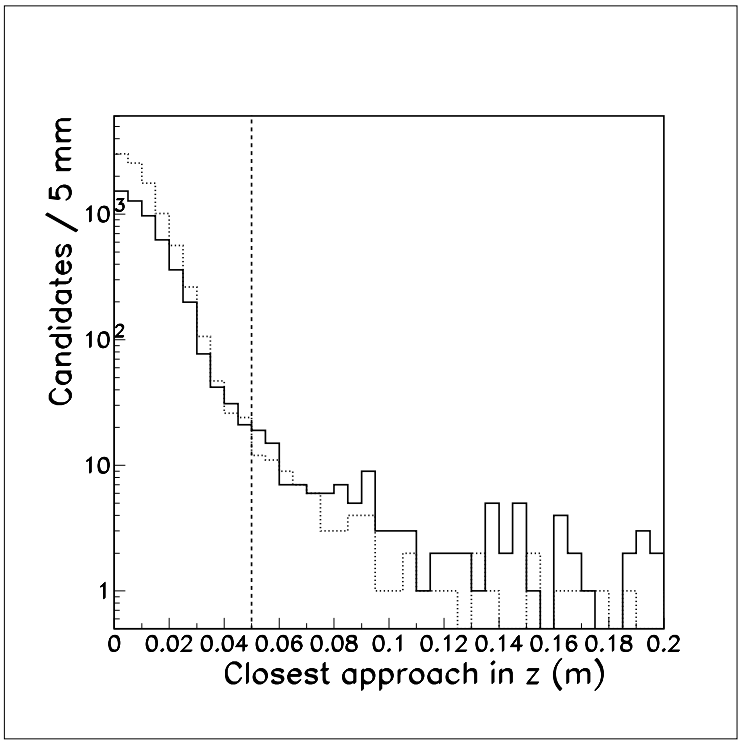


FIGURE 7. This is a plot of the absolute value of the distance of closest approach of the track to the interaction point in $z$, in meters. The solid line represents background events, and the dashed line represents signal events. The vertical dashed line indicates where we placed our cut, at 5 cm.

(the candidate mass of the $D^0$); and $M_{\pi^+}$ is the known mass of the $\pi^+_{\rm slow}$. For a $D^{*+}$ decay to a $D^0$ and a $\pi^+_{\rm slow}$, $Q$ should equal 5.9 MeV.

We used the Q distribution from the Monte Carlo simulated data for the $K^0_S\pi^0$ decay mode, shown in Fig. 8 without the cuts on significance of decay length and $\chi^2$ of the $K^0_S$ daughters to come from the beam spot, to determine the total number of signal events we had. We saw a peak at Q = 5.9 MeV, as expected. At first glance, we said the peak corresponded to signal events, and the relatively flat distribution underneath the peak corresponded to background. We fit the signal peak in $Q$ to two Gaussian functions, and obtained the weighted standard deviation $\sigma$ of 1 MeV. We then defined our signal region as 3.3 MeV < Q < 8.3 MeV, a width of about $2.5\sigma$ on either side of the known value of Q, and we said the events in the peak within that range were the signal events.

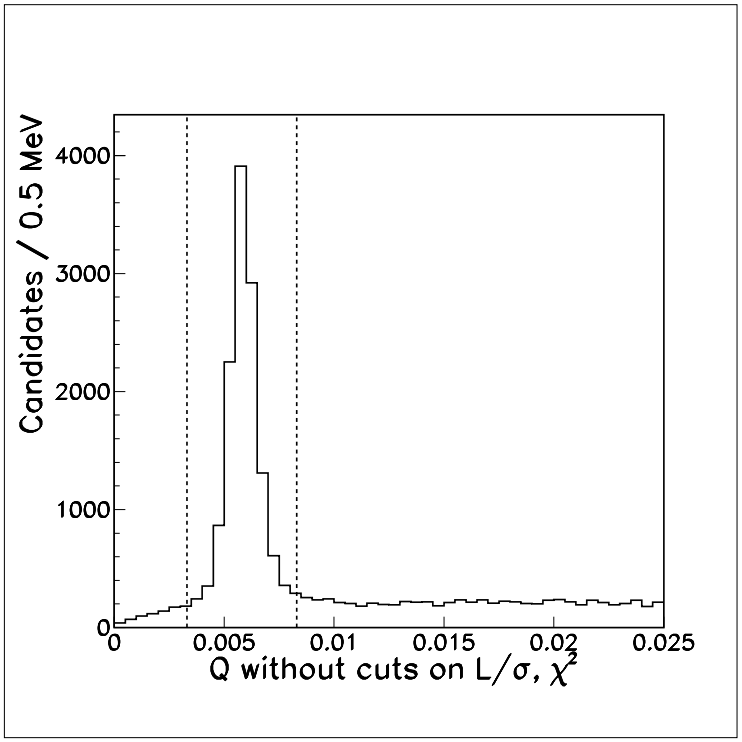


FIGURE 8. This is the Q distribution (in GeV) for the $K^0_S\pi^0$ decay mode without the cuts on significance of decay length and $\chi^2$ of the $K^0_S$ daughters to come from the beam spot. The vertical dashed lines define the signal region.

However, when we looked more deeply, we realized that there could be background events that peaked at $Q \approx 5.9$ MeV. There were basically two kinds of background present in our data sample. The first kind was combinatoric background; this was background due to the incorrect pairing of particles, from both real and fake $K^0_S$ and $\pi^0$. Combinatoric background was uniformly distributed, though, and so could be fit and accounted for.

The other type of background was from real $D^0$ mesons that decayed to modes other than our signal mode. For example, the $D^0$ could decay to modes such as $K^0_S\pi^0X$, where $X$ is some other particle or particles that we didn't detect. However, because we miss some of the decay products of the $D^0$ in this case, we always come up short in $D^0$ candidate

mass. Therefore, we're confident that this type of background will always be eliminated by accepting only events within a certain range of the nominal $D^0$ mass. This is illustrated in Fig. 9. The top distribution is a plot of $Q$ versus $M(K^0_S\pi^0)$ after all selection criteria except those based on the significance of decay length of the $K^0_S$ and the $\chi^2$ of the $K^0_S$ daughters to come from the beam spot were applied. Plot (a) in Fig. 9 shows background due to $D^0$ decay modes $K^0_S\pi^0X$; the events were almost all below our signal region, indicated by the box, in the candidate mass of the $D^0$.

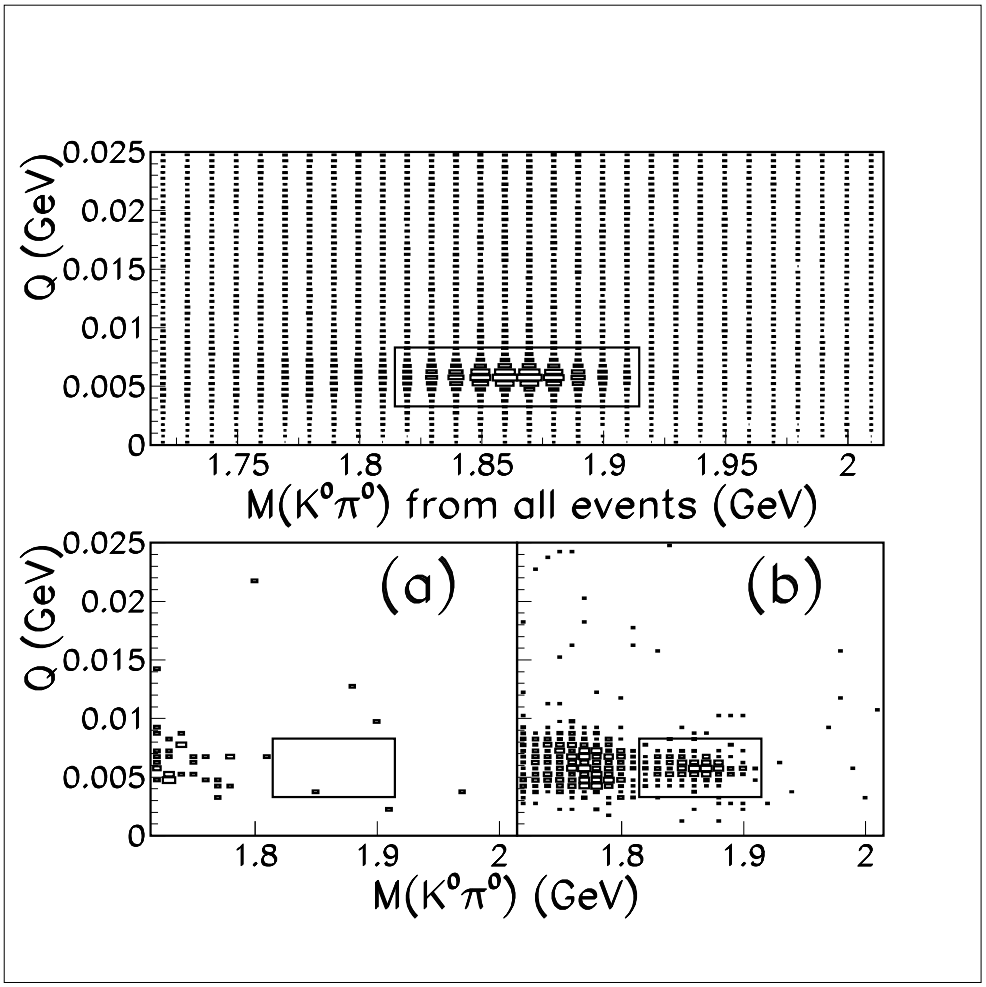


FIGURE 9. These are plots of $Q$ vs. $M(K^0_S\pi^0)$, in GeV, before the cuts on the significance of decay length of the $K^0_S$ and the $\chi^2$ of the $K^0_S$ daughters to come from the beam spot. The boxes delineate the signal region. The top distribution is for all events. Plot (a) displays background due to $D^0$ decay modes $K^0_S\pi^0X$. Plot (b) displays background due to $D^0$ decay modes $h^+h^-\pi^0$.

More worrisome in the data analysis are background modes like $h^+h^-\pi^0$, where $h^+$ and $h^-$ are some charged particles that didn't come from a $K^0_S$. We see all the products of this kind of decay, so we correctly reconstruct the $D^0$ mass. If the $D^0$ actually came from a $D^{*+}$, we will have the correct value of $Q$, also. As illustrated in plot (b) of Fig. 9, this type of background actually peaks in our signal region, and we needed to make sure we got rid of it.

The selection criteria based on the significance of the $K^0_S$ decay length and the $\chi^2$ of the $K^0_S$ daughters to come from the beam spot strongly suppressed background from other $D^0$ decay modes. This was true because those selection criteria eliminated events where the $D^0$ decayed immediately to charged particles. We used information from the Monte Carlo simulation about what particles were created in order to check how well we suppressed background from other $D^0$ decay modes, and found that this type of background was reduced to only 0.2% of the number of signal events within our signal region.

We can perform a similar check in the analysis of the real data, when we don't have the luxury of knowing the identity of the particles in question. The important observation here is that for any particular identity of $h^+$ and $h^-$, their invariant mass should be evenly distributed, at least near the $K^0_S$ mass. If we look at $K^0_S$ candidate mass, we should see a flat level of background due to modes such as $h^+h^-\pi^0$. This prediction was confirmed in the Monte Carlo data. So we can measure the level of this background outside of our signal region in $K^0_S$ candidate mass. Then we can use the fact that the background is flat to calculate how much background of this type falls within our signal region. Therefore, we are confident that we can check the remaining level of background from $D^0$ in the data after we apply our selection criteria, and correct for it in our analysis. This check and correction have yet to be performed.

Once the background was accounted for, the asymmetry in the decays of $D^0$ and $\overline{D^0}$ to the final state $K^0_S\pi^0$ was calculated in two different ways. The first way was to split the $Q$ distribution into two separate distributions. One distribution, which we called $Q_+$, was the $Q$ distribution for events "tagged" with $\pi^+_{\rm slow}$; these were the events with $D^0$ decays. The other distribution, which we called $Q_-$, was the $Q$ distribution for events tagged with $\pi^-_{\rm slow}$; these were the events with $\overline{D^0}$ decays. The $Q_+$ and $Q_-$ distributions for $K^0_S\pi^0$ in the simulated data are displayed in Fig. 10.

Once we created the $Q_+$ and $Q_-$ distributions, we fit the remaining background in each distribution to a threshold function with the exclusion of the signal region. An example of a fit, obtained from the analysis package MNFIT, is shown in Fig. 11; this is the fit to the total $Q$ distribution for this mode, but is illustrative of the technique. The fit information displayed at the top of the plot indicates how well the threshold function models the background.

Next, we interpolated the fit into the signal region of each distribution, and counted both the total number of events, $N$, and the number of background events, $B$, in the region. This allowed us to calculate $S_+(S_-)$, the number of signal events for the $Q_+(Q_-)$ distribution, according to the relationship $S = N - B$. Now, $S_+$ is actually equal to the number of $D^0$ that decayed to our signal mode $K^0_S\pi^0$; similarly, $S_-$ is equal to the number of $\overline{D^0}$ that decayed to $K^0_S\pi^0$. Therefore, Eq. (1) for the asymmetry may be rewritten as

$$\mathcal{A} = \frac{S_+ - S_-}{S_+ + S_-}. \tag{3}$$

We were most interested, though, not just in the value of the asymmetry, but in its uncertainty. The uncertainty in the asymmetry, $\sigma_{\mathcal{A}}$, may be calculated through standard error propagation techniques. It is given by the expression

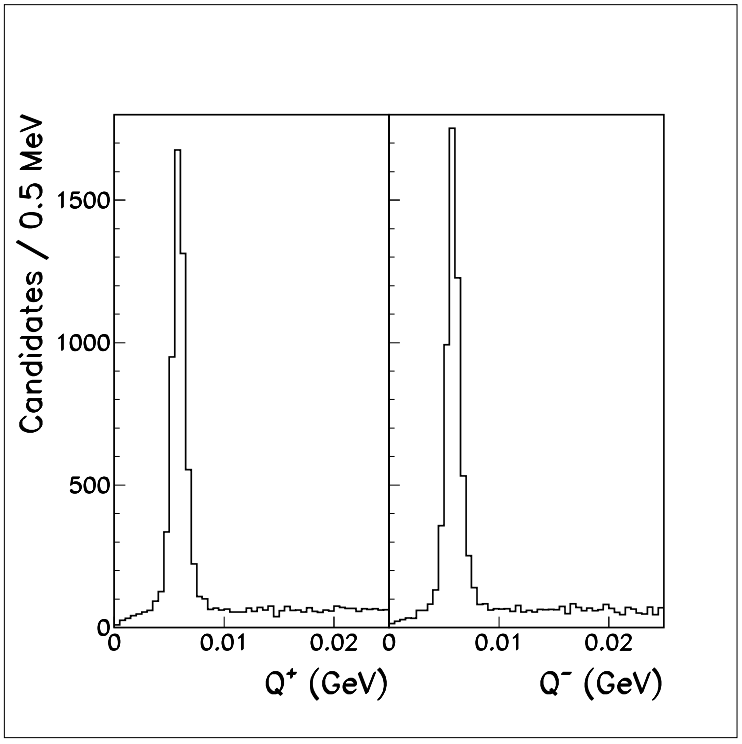


FIGURE 10. These are the plots of $Q_+$ and $Q_-$, in GeV, for Monte Carlo $K^0_S\pi^0$.

$$\sigma_{\mathcal{A}} = \sqrt{\frac{(1-\mathcal{A})\sigma_+}{S_+ + S_-} \oplus \frac{(1+\mathcal{A})\sigma_-}{S_+ + S_-}}, \tag{4}$$

where $\sigma_+(\sigma_-)$ is the uncertainty on $S_+(S_-)$. (The symbol $\oplus$ means to add in quadrature.) The important thing to notice is that the uncertainty is proportional to the reciprocal of the total number of signal events, $S_+ + S_-$. The more signal events we have, the lower the uncertainty on our measurement of $\mathcal{A}$ will be.

The second way to obtain the asymmetry was to first fit and count the background in the total Q distribution for the decay mode; the total $Q$ distribution is displayed in Fig. 12. We then counted the total number of events in the signal region, and obtained the total number of signal events. This gave us a direct measure of $S_+ + S_-$; in other words, we measured the denominator $S$ of the asymmetry calculation directly. Next, we subtracted $Q_+$ and $Q_-$ to obtain a distribution that was the difference between them; the difference histogram for $K^0_S\pi^0$ is also shown in Fig. 12. Then we counted the number of events in the signal region of this histogram. This in turn gave us a direct measure of $S_+ - S_-$; in other words, we also measured the numerator $\Delta S$ of the asymmetry directly. The difference histogram also provided a visual check that the background to our signal mode is symmetric; there was no significant difference between $Q_+$ and $Q_-$ in the background regions.

We may express the asymmetry in terms of the numerator and denominator that we obtained:

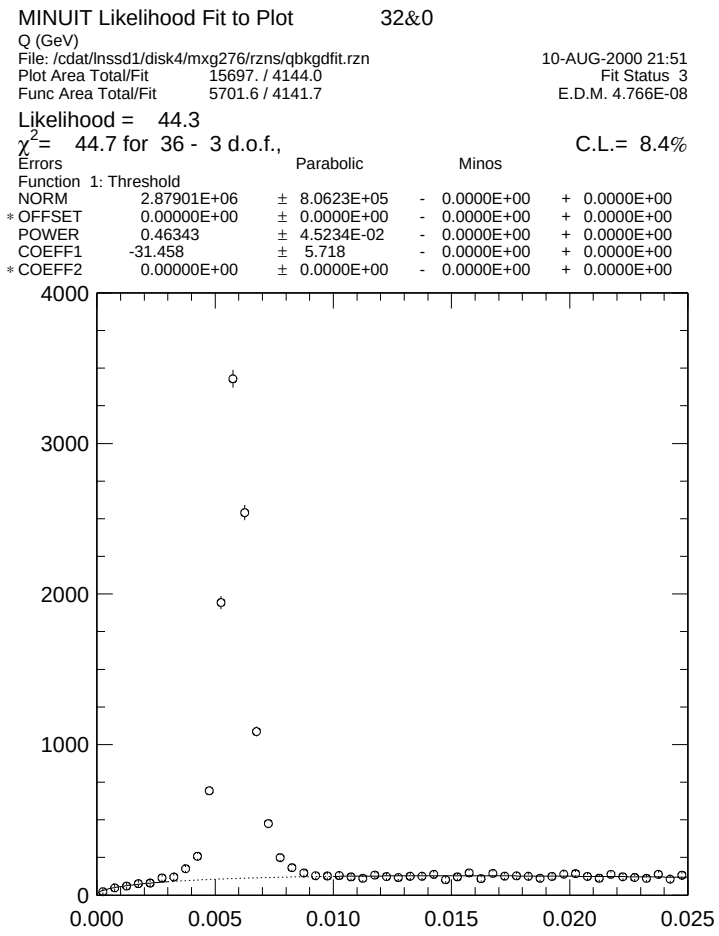


FIGURE 11. This figure displays the background fit for the total $Q$ distribution for $K^0_S\pi^0$. The fit information at the top of the figure indicates the high quality of the fit. The units are GeV.

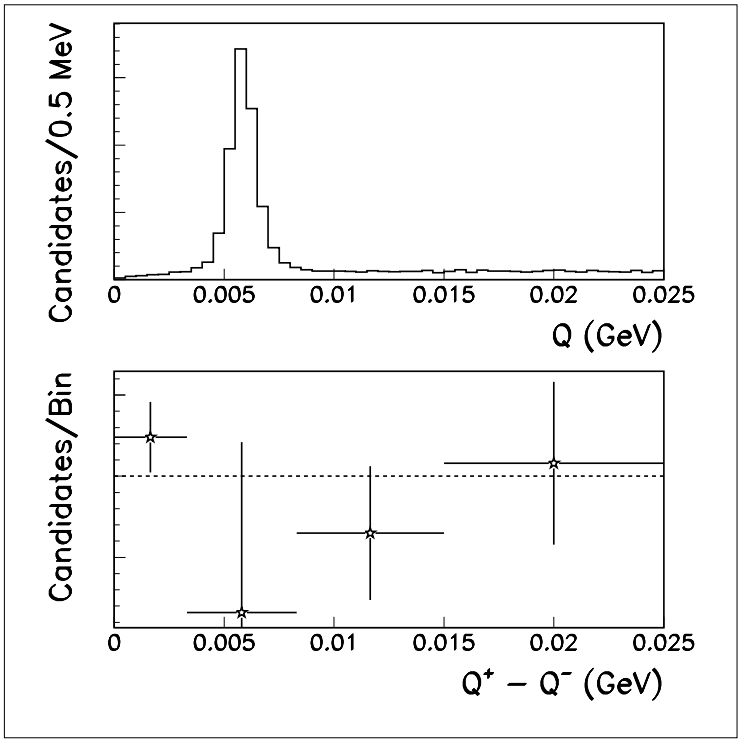


FIGURE 12. The upper distribution is the total $Q$ distribution for $K^0_S\pi^0$, in units of GeV. The lower distribution is the difference histogram, $Q^+ - Q^-$, or $\Delta S$, in units of GeV.

$$\mathcal{A} = \frac{\Delta S}{S}. \tag{5}$$

The uncertainty of the asymmetry for this method of calculation, obtained by propagation of error, is given by

$$\sigma_{\mathcal{A}} = \frac{\sqrt{4N_+N_-(S-B) + B^2(S+B) + \Delta S^2\sigma_B^2}}{S^2}, \tag{6}$$

where $N_+(N_-)$ is the total number of events in the signal region of $Q_+(Q_-)$, $B$ is the number of background events in the signal region of $Q$, and $\sigma_B$ is the uncertainty of $B$. This uncertainty has an inverse square relationship to the total number of signal events, so we expected this method to give a lower uncertainty than the first method when few signal events were present.

Once our analytic machinery was assembled, we applied both methods of calculating the asymmetry to our Monte Carlo simulated data. The Monte Carlo data was created to have zero asymmetry, since we expected the asymmetry in the real data to be very small. This feature provided an easy check of our calculations for the simulated data; all the asymmetries we measured should be consistent with zero.

The results of calculating the asymmetry in the Monte Carlo data with the first method, obtaining $S_+$ and $S_-$ separately, are shown in Table 2. The results from applying the second method, obtaining the numerator and denominator of the asymmetry directly, are shown in Table 3. As expected, the asymmetries given by both methods were consistent with zero.

TABLE 2. Results of the first method of asymmetry calculation in the Monte Carlo data, obtaining $S_+$ and $S_-$ separately, for all three signal modes.

| Decay mode | A | $\sigma_{\mathcal{A}}$ |
|---|---|---|
| $K^0_S\pi^0$ | $-0.4\%$ | $1.1\%$ |
| $K^0_S K^0_S$ | $-8.0\%$ | $9.9\%$ |
| $\pi^0\pi^0$ | $-4.8\%$ | $4.8\%$ |

TABLE 3. Results of the second method of asymmetry calculation in the Monte Carlo data, obtaining the numerator and denominator of the asymmetry directly, for all three signal modes.

| Decay mode | A | $\sigma_{\mathcal{A}}$ |
|---|---|---|
| $K^0_S\pi^0$ | $-0.8\%$ | $1.1\%$ |
| $K^0_S K^0_S$ | $-6.3\%$ | $9.7\%$ |
| $\pi^0\pi^0$ | $-8.7\%$ | $4.7\%$ |

These results and the results for the decay modes $K^0_S K^0_S$ and $K^0_S\pi^0$ (discussed below) made us confident that our analysis methods were reasonable; the asymmetries were consistent with zero, the uncertainties were low, and we had a large number of signal events to work with (see Table 6 for the $K^0_S\pi^0$ decay mode). Therefore, we applied our analysis to the real data

samples. We obtained the preliminary results displayed in Table 4 (for the first method) and Table 5 (for the second method). We saw that the asymmetry in the decays of $D^0$ and $\overline{D^0}$ to the final state $K^0_S\pi^0$ was consistent with zero, in line with the predictions of the Standard Model. There does not seem to be any new physics at work. Note that these results are only preliminary, as some work remains to be done in the analysis. We still must check how well background from real $D^0$ is suppressed in the data, correct for systematic uncertainties, and examine the two data sets CLEOII and CLEOII.V separately before these results may be considered final.

TABLE 4. Results of the first method of asymmetry calculation in the real data, obtaining $S_+$ and $S_-$ separately, for all three signal modes. These results are preliminary.

| Decay mode | A | $\sigma_{\mathcal{A}}$ |
|---|---|---|
| $K^0_S\pi^0$ | $-0.1\%$ | $1.1\%$ |
| $K^0_S K^0_S$ | $-15.6\%$ | $15.6\%$ |
| $\pi^0\pi^0$ | $-4.3\%$ | $5.0\%$ |

TABLE 5. Results of the second method of asymmetry calculation in the real data, obtaining the numerator and denominator of the asymmetry directly, for all three signal modes. These results are preliminary.

| Decay mode | A | $\sigma_{\mathcal{A}}$ |
|---|---|---|
| $K^0_S\pi^0$ | $-0.3\%$ | $1.1\%$ |
| $K^0_S K^0_S$ | $-13.3\%$ | $14.9\%$ |
| $\pi^0\pi^0$ | $-0.4\%$ | $4.9\%$ |

TABLE 6. This table displays the total number of events $N$, the number of background events $B$, the number of signal events $S$, and the difference in the number of $D^0$ and $\overline{D^0}$ $\Delta S$ within the signal region in $Q$ after all selection criteria were applied. These numbers are for the $K^0_S\pi^0$ mode; both Monte Carlo and real data results are displayed.

| Decay mode | Monte Carlo | Data |
|---|---|---|
| $N$ | $11030 \pm 105$ | $9733 \pm 99$ |
| $B$ | $1089 \pm 6$ | $938 \pm 6$ |
| $S$ | $9941 \pm 105$ | $8795 \pm 99$ |
| $\Delta S$ | $-81 \pm 105$ | $-23 \pm 99$ |

## $D^0/\overline{D^0} \to K^0_S K^0_S$

Our selection criteria for the particles involved in this decay were determined in the same manner as for the $K^0_S\pi^0$ decay mode. The selection criteria for the $K^0_S K^0_S$ signal mode are shown in Table 1. The mass restrictions for the $K^0_S$ and $D^0$ candidates were tighter than they were for the $K^0_S\pi^0$ mode. We had better resolution for this mode, because both the $D^0$

daughters decayed into charged particles that we see in the detector. Therefore, the signal peaks were narrower.

We also checked how well we were able to suppress background modes due to real $D^0$. Once the selection criteria were applied, we found that this type of background was present at only 3.0% of the signal level within our signal region. Then we calculated the asymmetry in two different ways for the Monte Carlo data. As shown in Table 2 and Table 3, the asymmetries were also consistent with zero, as they should be. Notice that for this mode, the second method of obtaining the numerator and the denominator of the asymmetry directly gave a lower uncertainty than the first method. The $K^0_S K^0_S$ mode has a smaller branching fraction ($6.5 \pm 2.0\ 10^{-4}$) than the other two signal modes ($1.06 \pm 0.11$ % for $K^0_S\pi^0$ and $8.4 \pm 2.2\ 10^{-4}$ for $K^0_S K^0_S$), which means it occurs less frequently and we have less data to work with. This is illustrated by Table 7, which shows the numbers of events we had after applying our selection criteria; a comparison of this table to Table 6 (for $K^0_S\pi^0$) and Table 8 (for $\pi^0\pi^0$) shows that we did indeed have fewer events to work with. The results of our asymmetry calculation indicate that in such a case of low statistics, the second method of calculating the asymmetry is preferable.

TABLE 7. This table displays the total number of events $N$, the number of background events $B$, the number of signal events $S$, and the difference in the number of $D^0$ and $\overline{D^0}$ $\Delta S$ within the signal region in $Q$ after all selection criteria were applied. These numbers are for the $K^0_S K^0_S$ mode; both Monte Carlo and real data results are displayed.

| Decay mode | Monte Carlo | Data |
|---|---|---|
| $N$ | $152 \pm 12$ | $81 \pm 9$ |
| $B$ | $25 \pm 3$ | $21 \pm 2$ |
| $S$ | $127 \pm 13$ | $60 \pm 9$ |
| $\Delta S$ | $-8 \pm 12$ | $-8 \pm 9$ |

The preliminary results for both methods of calculating the asymmetry in the real data are shown in Table 4 and Table 5. As expected, the second method gave a lower uncertainty for this rarer decay mode. However, notice that the uncertainties of the asymmetries in the data for this mode were considerably higher than they were for the simulated data. It's possible that we generated more signal events in the simulation than actually appeared in the data; this lack of signal manifested itself as a higher uncertainty. This effect was just more noticeable for the $K^0_S K^0_S$ mode, since there was a lower amount of signal to begin with. Further investigation into the simulation is necessary to explain this effect.

$$D^0/\overline{D^0} \rightarrow \pi^0\pi^0$$

Our selection criteria for the particles involved in this decay were again determined in the same manner as for the $K^0_S\pi^0$ decay mode. The selection criteria for the $\pi^0\pi^0$ signal mode are displayed in Table 1. Note that the situation here was the opposite of that for the $K^0_S K^0_S$ mode; we had worse resolution for this mode, where both the $D^0$ daughters decayed into photons, and so the signal peaks in mass were broader. This forced us to widen our mass selection window for the $\pi^0$ and $D^0$ candidates. Also note that the cut on the cosine of

the decay angle, here the angle between the $\pi^0$ momentum in the $D^0$ rest frame and the $D^0$ lab momentum, was much more severe than for $K^0_S\pi^0$ or $K^0_SK^0_S$ ; since both the $\pi^0$ and their daughters are neutral, we had less information to base our selection criteria on. Rejecting events based on the cosine of the decay angle was one of the few powerful ways we had to eliminate background to this mode.

Once the selection criteria were established, we again calculated the asymmetry in two different ways for the Monte Carlo data. As shown in Table 2 and Table 3, the asymmetries were again consistent with zero, as expected. The fact that the asymmetries were consistent with zero for all three modes in the Monte Carlo data gave us confidence that our analysis methods were valid. The preliminary results for both methods of calculating the asymmetry for this mode in the real data are shown in Table 4 and Table 5. Note that for this mode and the $K^0_S\pi^0$ mode, the two more prevalent signal modes, the two methods of asymmetry calculation were consistent with each other. A comparison of the values given in Table 8 to those given in Table 7 (for $K^0_SK^0_S$) confirms that this mode is more numerous than the $K^0_SK^0_S$ mode. So for high statistics, the two methods of calculating the asymmetry are essentially the same.

TABLE 8. This table displays the total number of events $N$, the number of background events $B$, the number of signal events $S$, and the difference in the number of $D^0$ and $\overline{D^0}$ $\Delta S$ within the signal region in $Q$ after all selection criteria were applied. These numbers are for the $\pi^0\pi^0$ mode; both Monte Carlo and real data results are displayed.

| Decay mode | Monte Carlo | Data |
|---|---|---|
| $N$ | 1342 ± 37 | 1447 ± 38 |
| $B$ | 564 ± 5 | 676 ± 5 |
| $S$ | 778 ± 37 | 771 ± 38 |
| $\Delta S$ | -68 ± 37 | -3 ± 38 |

## Systematic Error

In this analysis, we were concerned with systematic as well as statistical uncertainties. We wanted to make sure that our results were not biased due to factors that could be corrected for. One source of systematic uncertainty could be background from other decay modes of the $D^0$. Such background modes can in fact show up in the signal region; if formed in a CP violating process, and not removed or accounted for, such background modes could cause us to falsely measure an asymmetry. However, as discussed in the sections on the $K^0_S\pi^0$ and $K^0_SK^0_S$ decay modes, we were able to strongly suppress this kind of background in the Monte Carlo simulated data. (Background from real $D^0$ mesons does not show up in the signal region for the $\pi^0\pi^0$ decay mode.) In addition, we can check for background from real $D^0$ mesons in the data, and correct for it, as discussed above.

The other possible source of systematic uncertainty in our analysis is the presence of a bias in our selection of the slow pions that come from the $D^{*+}$ decay. The charge of the slow pion from the decay $D^{*+} \rightarrow D^0\pi^+_{\rm slow}$ identifies or "tags" the initial state of the $D^0$. Reconstruction- and detector-induced effects can produce an apparent asymmetry in the

number of tagged $D^0$ and $\overline{D^0}$ mesons. An unbiased sample of $\pi^+_{slow}$ is selected with the track cuts described in the first section. We also accept only hadronic events with an event vertex near the $e^+e^-$ interaction point. The track selection criteria are identical for the CLEOII and CLEOII.V configurations; nonetheless, we measure the asymmetry separately for the two detector configurations.

The momentum range of $\pi^+_{slow}$ from $D^{*+}$ from $c\bar{c}$ events is distributed between 100 and 400 MeV. We measure the charge asymmetry for $\pi^\pm$ daughters of selected $K^0_S$ candidates for the momentum range 100 to 400 MeV. Both the $K^0_S$ daughters must pass the track selection criteria given above. The $K^0_S$ candidate vertex is required to be separated from the event vertex by at least three times the resolution on the $r\phi$ (3-dimensional) decay length for CLEOII (CLEOII.V). The selected $K^0_S$ candidates are shown in Fig. 13. The measured asymmetry ($\mathcal{A} \equiv (N_+ - N_-)/(N_+ + N_-)$) is shown in Fig. 14 as a function of the magnitude of the $\pi^+_{slow}$ momentum, $p(\pi^+_{slow})$, and the cosine of the polar angle of the $\pi^+_{slow}$, $\cos\Theta_{\pi^+_{slow}}$. We have corrected the asymmetry measured for $\pi^\pm$ from the $K^0_S$ peak region using the asymmetry measured in the $K^0_S$ sideband regions. No significant dependence on $p(\pi^+_{slow})$ or $\cos\Theta_{\pi^+_{slow}}$ is observed. Integrating over $\cos\Theta_{\pi^+_{slow}}$ for momenta 100-400 MeV, we measure $\mathcal{A}(\text{CLEOII}) = (-0.35\pm0.65)\%$ and $\mathcal{A}(\text{CLEOII.V}) = (+0.17\pm0.43)\%$. The luminosity-weighted average for the CLEOII and CLEOII.V configurations is $\mathcal{A} = (-0.01\pm0.36)\%$. We can therefore correct for this systematic error in our results. However, it is important to note that this source of error is insignificant compared to our statistical uncertainty.

## Conclusions

In conclusion, our preliminary results showed that the asymmetries between decays of $D^0$ and its antiparticle $\overline{D^0}$ to the final states $K^0_S\pi^0$, $K^0_SK^0_S$, and $\pi^0\pi^0$ were all consistent with zero, in agreement with predictions of the Standard Model. We also concluded that our second method of calculating the asymmetry, that of obtaining the numerator and denominator of the asymmetry directly, is the preferred method, as it performs better for lower statistics. Although we did not find evidence for new physics, we were able to make two new measurements (the asymmetries in decays to $K^0_SK^0_S$ and $\pi^0\pi^0$). We also improved the uncertainty on the previous measurement of $-1.3 \pm 3.0\%$ for the $K^0_S\pi^0$ mode by a factor of three.[1]

Some work remains before the data analysis results can be called final, though. The data from CLEOII and CLEOII.V need to be analyzed separately, since there should be a difference in our resolution for the two data sets. Also, we need to make sure that background modes from real $D^0$ are suppressed in the real data as well as they were in the simulated data. Any systematic uncertainties due to remaining background modes or to an asymmetry in our $\pi^+_{slow}$ selection must be corrected for. Finally, we must examine our simulation to confirm the branching ratios for the signal modes were modeled appropriately.

## Acknowledgments

We are pleased to acknowledge Dr. David Jaffe of the University of California at San Diego for proposing this Research Experience for Undergraduates project and for his invaluable support and guidance. We would also like to thank Dr. David Cassel of Cornell University and Dr. Hans Paar of the University of California at San Diego for their time

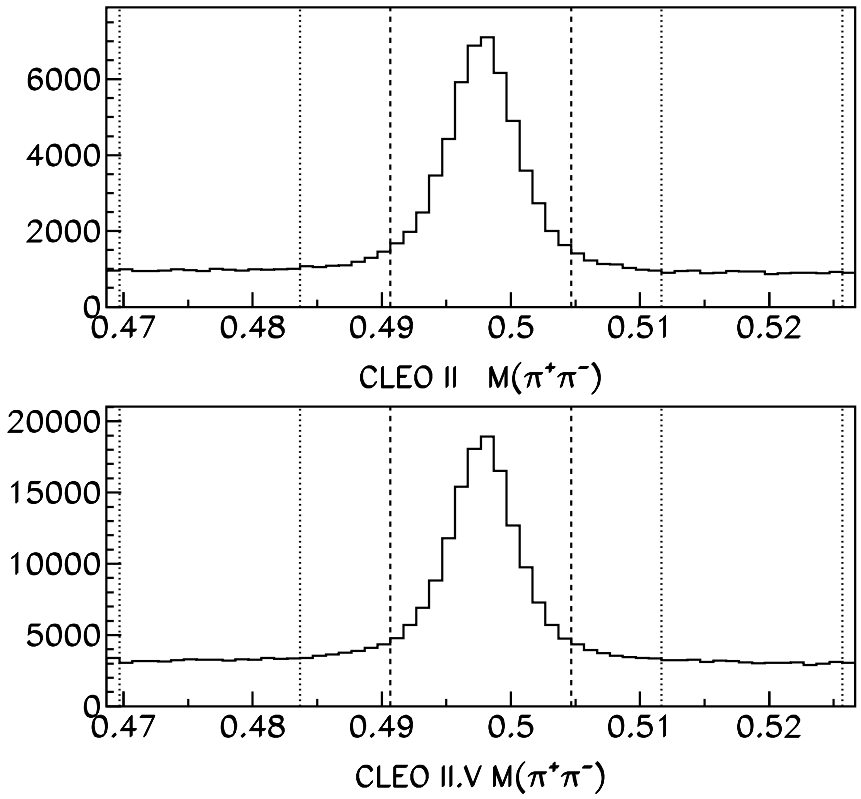


FIGURE 13. The $\pi^+\pi^-$ invariant mass spectrum of $K^0_S$ candidates used for determination of the asymmetry of the $\pi^+_{slow}$ selection criteria. The vertical dashed (dotted) lines indicate the peak (sideband regions). The upper (lower) plot is for CLEOII (CLEOII.V) data.

and help. Additionally, Larry Borum would like to thank Prof. Giovanni Bonvicini and Prof. David Cinabro of Wayne State University for their encouragement and assistance in the preparation for the project. This work was supported by National Science Foundation REU grant PHY-9731882 and research grants PHY-9809799 and PHY-9820306.

## Footnotes and References

1. The CLEO collaboration looked for CP violation in the decays $D^0 \to K^+K^-$, $K^0_S\phi$, $K^\mp\pi^\pm$, and our signal mode $K^0_S\pi^0$. CLEO Collaboration, J. Bartelt *et al.*, CLNS 95/1333. "Search for CP violation in $D^0$ decay." May 18, 1995.
2. We obtained all known masses and branching ratios from the Particle Data Group's publication. Particle Data Group, R. M. Barnett *et al.*, Physical Review D **54**, 1 (1996).

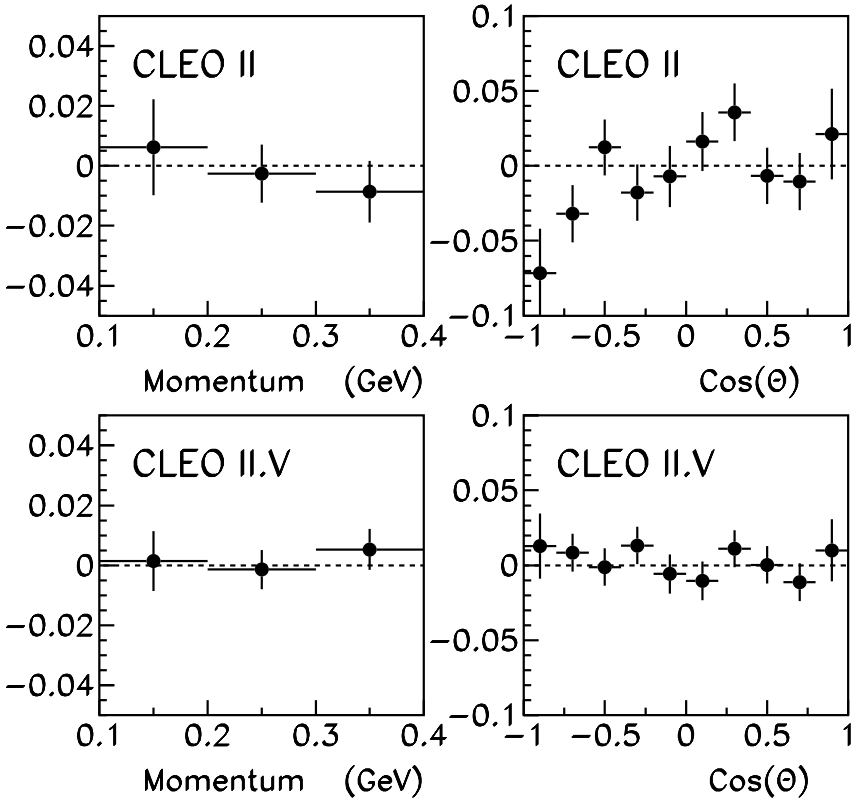


FIGURE 14. The measured asymmetry for $\pi^{\pm}$ daughters of $K^0_S$ candidates as a function of the pion momentum and cosine of the polar angle separately for CLEOII and CLEOII.V.